Water Practice & Technology

IWA PUBLISHING

Water Practice & Technology Vol 16 No 4, 1386 doi: 10.2166/wpt.2021.079

Water treatment with CoZnAl-LDH and its mixed metal oxide

Mina Sharifi-Bonab[a], Soheil Aber[a,*], Dariush Salari[b] and Fatemeh Khodam[a]

[a] Research Laboratory of Environmental Protection Technology (RLEPT), Department of Applied Chemistry, Faculty of Chemistry, University of Tabriz, Tabriz, Iran
[b] Department of Applied Chemistry, Faculty of Chemistry, University of Tabriz, Tabriz, Iran
*Corresponding author. E-mail: soheil_aber@yahoo.com; s_aber@tabrizu.ac.ir

ABSTRACT

CoZnAl-layered double hydroxide (LDH) was synthesized by homogeneous co-precipitation. CoZnAl-Mixed Metal Oxide (MMO) was prepared by calcining the LDH. The samples' structure and morphology were studied by analytical techniques including X-ray diffraction, N_2 adsorption-desorption isotherm, scanning electron microscopy and UV–visible spectroscopy. Acid orange 7 (AO7) adsorption by as-prepared samples was studied. CoZnAl-MMO showed 526.32 mg/g adsorption capacity, higher than that of CoZnAl-LDH, 243.9 mg/g. Kinetic studies confirmed the pseudo-second-order and pseudo-first-order AO7 adsorption kinetics of the LDH and MMO, respectively. AO7 adsorption onto both LDH and MMO fitted the Langmuir isotherm model well. Band gap calculation confirmed the ability of this nano-MMO to operate in the visible light region. It displayed synergetic adsorption-photocatalytic performance under visible light and the removal efficiency was about 97%.

Key words: adsorption, layered double hydroxide, mixed metal oxide, photocatalysis

HIGHLIGHTS

- The CoZnAl-LDH with high surface area was synthesized.
- The LDH adsorbed acid orange 7 from aqueous solution effectively.
- The CoZnAl-MMO was prepared via calcination of the CoZnAl-LDH.
- The MMO showed photocatalytic activity in visible light and high adsorption capacity towards AO7.

GRAPHICAL ABSTRACT

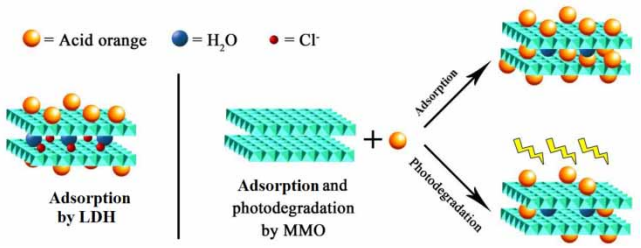

INTRODUCTION

Many studies have been done into the potential use of layered double hydroxides (LDHs) in wastewater treatment. LDHs application is increasing day by day due to their special properties, including large specific surface, the ability to remove organic and inorganic species, easy and inexpensive synthesis, and the possibility of producing diverse LDH species with different metals and interlayer anions for different applications (Mostafa *et al.* 2016).

LDHs consist of positive metal hydroxide layers and interlayer anions. Their general formula is written as:

$$[M(II)_{(1-x)}M(III)_x(OH)_2]^{x+}\left[(A_n)_{\frac{x}{n}}.m(H_2O)\right]^{x-}$$

where $M(II)$ and $M(III)$ are divalent and trivalent metals and A^{n-} is an anion.

Such structures enable the synthesis of LDHs with different metals and interlayer anions suitable for diverse applications as catalysts (Xu *et al.* 2011), catalyst supports (Kovanda & Jirátová 2011), adsorbents (Rathee *et al.* 2020), scavengers (Kong *et al.* 2019), electrocatalysts (Speed 2016) and photocatalysts (Li *et al.* 2020).

Adsorption has been used to remove various pollutants, especially heavy metals and synthetic dyes, because of properties such as low cost, lack of toxic byproducts, simple design for large-scale use and high removal efficiency (Patra *et al.* 2016). Materials including zeolites, carbon compounds, resins, biomaterials, and polymers are used to remove dyes. LDHs are also considered as adsorbents, today, because of their special properties.

LDHs remove solutes from water via two mechanisms – adsorption onto their positively charged layers and, alternatively, by anion exchange and intercalation (Ahmed & Mohamed 2017).

Photocatalysis is an advanced oxidation process that works on the basis of producing hydroxyl radicals ($^{\cdot}OH$) with high oxidation potential (E = 2.8 V/SHE), which can oxidize a wide range of organic compounds. In recent decades, TiO_2 and ZnO have received attention as non-toxic, stable, low-cost and efficient photocatalysts. Due to their large energy band gaps, they are only active under ultraviolet light (Yu *et al.* 2016), which limits their widespread use due to high energy consumption.

LDHs, and the mixed metal oxides (MMOs) obtained by their calcination and active as photocatalysts in visible light, have been studied in dye removal, with reports of them acting as adsorbents and photocatalysts simultaneously. Morimoto et al. (2011) surveyed anionic dye removal by ZnAl-LDH and MgAl-LDH, via adsorption and photodegradation mechanisms. LDH composites have also been introduced as adsorbents and photocatalysts (Yu *et al.* 2016; Li *et al.* 2017).

In this work, CoZnAl-LDH was prepared by easy and inexpensive co-precipitation, and its adsorption capacity for acid orange 7 (AO7) removal investigated. The adsorption and photocatalytic properties of CoZnAl-MMO, obtained by thermal treatment of the LDH, were also investigated.

MATERIALS AND METHODS

Materials

$ZnCl_2.6H_2O$, $CoCl_2.6H_2O$, and $AlCl_3.6H_2O$ were purchased from the Merck Company. AO7 was obtained from the local market – its characteristics are presented in Table 1. Solution pH values were adjusted using 0.1 M solutions of HCl or NaOH, as appropriate. All reagents were used without further treatment and distilled water was used both in synthesis and to wash the precipitates.

Table 1 | Characteristics of AO7 (Abdollahi *et al.* 2018)

Structure	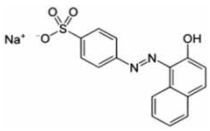
Chemical formula	$C_{16}H_{11}N_2NaO_4S$ (sodium salt)
Chemical class	Azo
λ_{max} (nm)	484

CoZnAl-LDH synthesis

The CoZnAl-LDH was synthesized by co-precipitation. The appropriate amounts of $CoCl_2.6H_2O$, $ZnCl_2.6H_2O$, and $AlCl_3$ (on the basis that Co:Zn:Al should be 1:1:1) were dissolved in 40 ml of distilled water subject to constant stirring with a magnetic stirrer. The correct proportion of a 3 M solution of NaOH was added to bring the pH to 10 and the solution was then maintained at 60°C for 24 hours. The precipitate was separated by centrifugation, washed twice and then dried at 40 °C. The MMO was obtained by calcining the LDH at 300 °C for 3 hours.

Characterization

XRD patterns of the as-prepared samples were obtained using a Bruker AXS (Germany) model D8 advanced diffractometer for CuK_α radiation ($\lambda = 1.54\ ^\circ A$). Sample morphology was studied by field emission scanning electron microscopy (FESEM) (ULTRA55, Carl Zeiss MST AG, Germany). The Brunauer Emmett Teller (BET) surface

area measurements were done using a Quantachrome chemBET device. The samples' UV–vis absorbance was recorded using a T80^{+} UV/VIS Spectrometer (PG Instruments Ltd, UK), and that of the solutions, against water at 484 nm, with a Perkin-Elmer 550 SE spectrophotometer.

Point of zero charge (PZC) of CoZnAl-LDH and CoZnAl-MMO

The point of zero charge (PZC) of the samples was determined in 0.1 M $NaNO_3$ solution at room temperature. 20 ml aliquots of the $NaNO_3$ solution were placed in five titration flasks and their pHs adjusted to 4 to 9 using 0.1 M HNO_3 and NaOH solutions using a pH meter (Eutech pH 510, Malaysia). 0.1 g sample aliquots were poured into each flask and shaken for 24 hours in a shaker-incubator, after which the pH was measured. The difference between the initial and final solution pH (ΔpH) was plotted against the initial pH (pH_i) values. The PZC was estimated from the plot as the pH at which ΔpH was equal to zero (Mahdizadeh & Aber 2015).

Adsorption experiments

Batch adsorption experiments were done in the dark and at room temperature. In order to identify the adsorption isotherm of the process, 10 mg of CoZnAl-LDH or CoZnAl-MMO were agitated in 50 mL AO7 solution for 24 hours with dye concentrations of 40 to 100 mg/L for LDH experiments and 80 to 120 mg/L for MMO.

The adsorption kinetic model of the samples, as synthesized, was determined by putting 10 mg of adsorbent into 50 mL AO7 solution with dye concentrations of 30 to 80 mg/L for LDH experiments and 80 to 120 mg/L for MMO, and taking samples at regular intervals. Solution absorbance was measured by UV-vis spectrophotometer at 484 nm, which is the maximum absorbance wavelength for AO7. An AO7 calibration diagram was used to calculate dye concentration.

The removal proportion (R%) of the pollutant is defined by Equation (1):

$$R = \frac{C_0 - C_t}{C_0} \times 100 \tag{1}$$

where C_0 and C_t (both mg/L) are the initial and final concentrations of AO7, respectively.

The adsorption capacity at equilibrium condition q_e (mg/g) is expressed by Equation (2):

$$q_e = \frac{C_0 - C_e}{M} \times V \tag{2}$$

where V is the dye solution volume (L), C_0 the initial AO7 concentration (mg/L), C_e the dye concentration at equilibrium (mg/L), and M the adsorbent mass (g).

Photodegradation experiments

To consider the photodegradation efficiency of the MMO, as-prepared, AO7 was degraded in a photoreactor equipped with a 45 W visible-light lamp (CCP, Iran). The contributions of the adsorption and photodegradation mechanisms were determined by conducting the experiments simultaneously. The difference between the diagrams in the dark and under light was taken as being the photodegradation removal. All tests were performed twice and, for all points, error bars were drawn based on the standard deviation.

RESULTS AND DISCUSSION

Structural characterization

The XRD analyses of CoZnAl-LDH and CoZnAl-MMO proved their successful synthesis, and the characteristic reflections of the LDH structure are visible (Figure 1). The peaks at 12, 23.5, 35, and 60.5° could be indexed as (003), (006), (110) and (113), which are typical reflections of the hydrotalcite-like structure (JCPDS No 15-0.087) (Xu *et al.* 2014). In forming CoZnAl-MMO, the layered structure of CoZnAl-LDH is destroyed so the related peaks disappear. Most peaks in the MMO XRD pattern are related to ZnO (JCPDS card No 36-1451). Because of the low calcination temperature (300 °C) of CoZnAl-LDH, it is not possible to form oxides of cobalt or aluminum (Klemkaite *et al.* 2011). Increasing the LDH calcination temperature leads to increased MMO particle size, which reduces its adsorption capacity and photocatalytic activity.

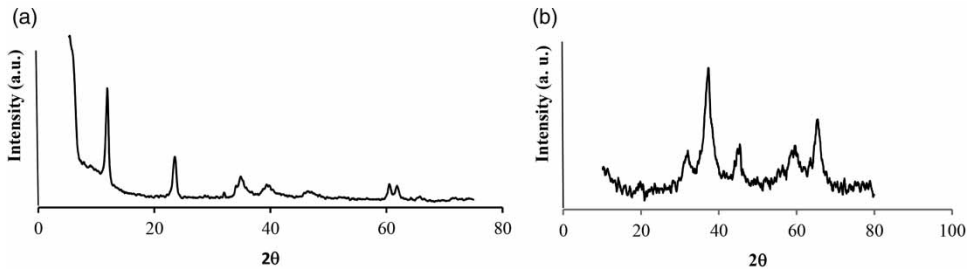

Figure 1 | XRD patterns of (a) CoZnAl-LDH and (b) CoZnAl-MMO.

The morphology of the LDH and MMO was characterized by SEM coupled with energy-dispersive X-ray spectroscopy (EDS) analysis. As can be seen in Figure 2, the synthesized CoZnAl-LDH and CoZnAl-MMO consist of uniform spherical particles, with average diameters of 10 to 20 and 20 to 30 nm, respectively.

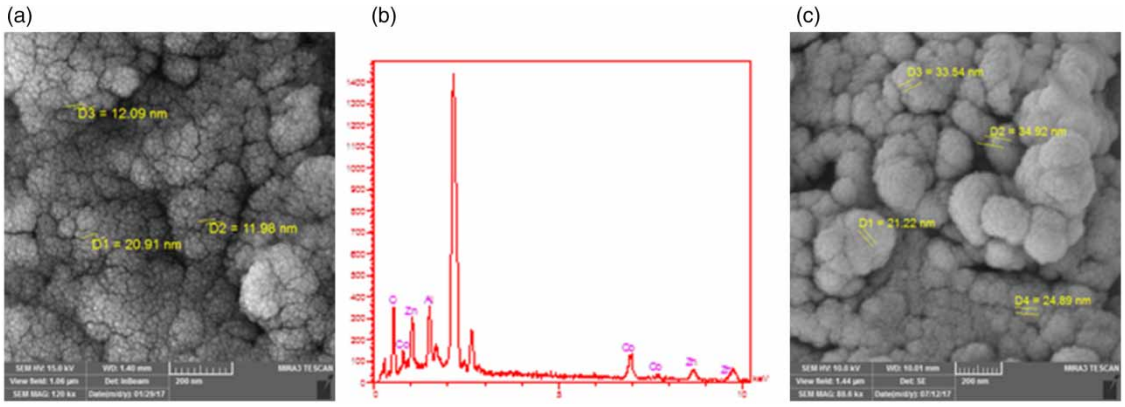

Figure 2 | SEM image of CoZnAl-LDH (a), EDS analyses of CoZnAl-LDH (b) and SEM image of CoZnAl-MMO (c).

The EDS plot for the LDH is shown in Figure 2(b). The X-ray energies related to Co, Zn, Al and O are distinctive, providing further evidence for successful CoZnAl-LDH synthesis. Figure 3(a) and 3(b) show the samples' nitrogen adsorption-desorption isotherms. Both isotherms belong to type IV with an H_3 hysteresis loop, showing that they have a layered structure, which is a characteristic of LDHs and LDH-derived MMOs. On the other hand, both samples contain mesopores, as a characteristic of type IV isotherm (Thommes *et al.* 2015).

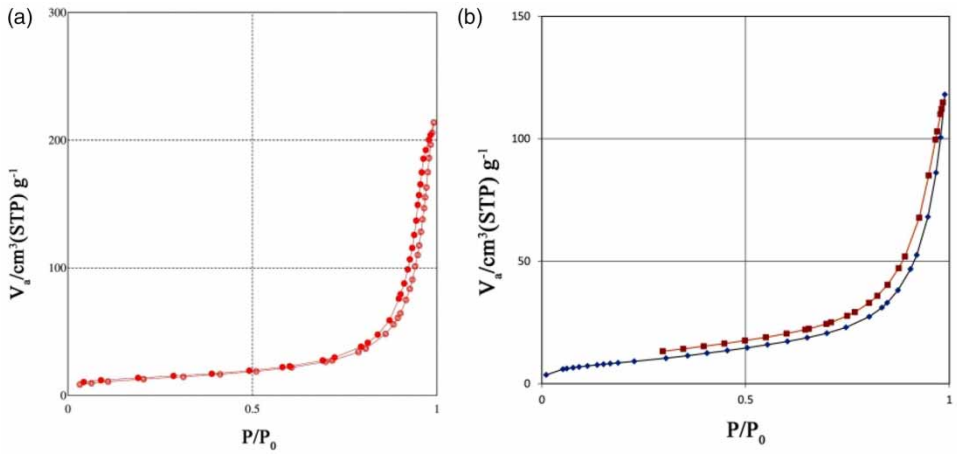

Figure 3 | N_2 adsorption-desorption isotherms of CoZnAl-LDH (a) and CoZnAl-MMO (b).

Table 2 shows the specific surface, average pore size and total pore volume of the samples. The high specific surface of the samples with the positive surface charge leads to the good adsorption of the anionic dye by these materials.

Table 2 | Sample textural properties

Sample	BET surface (m^2/g)	Pore volume (cm^3/g)	Pore size (nm)
CoZnAl-LDH	44.876	10.310	29.048
CoZnAl-MMO	33.112	7.6077	22.054

The sample absorption spectra are shown in Figure 4(a). The absorption intensity of CoZnAl-LDH was weaker than that of CoZnAl-MMO in visible light. Furthermore, LDH showed one absorption edge around 200 nm, while MMO showed two around 250 and 382 nm. This indicates that visible light can cause electron transfer from the valence to the conducting band of CoZnAl-MMO. To determine the optical band gap, the Davis and Mott model was applied (Davis & Mott 1970), and calculated using Equation (3):

$$ahv = D(hv - E_g)^n \tag{3}$$

where a is absorbance, hv the photon energy, E_g the optical band gap, and $n = 1/2$ for allowed direct transition.

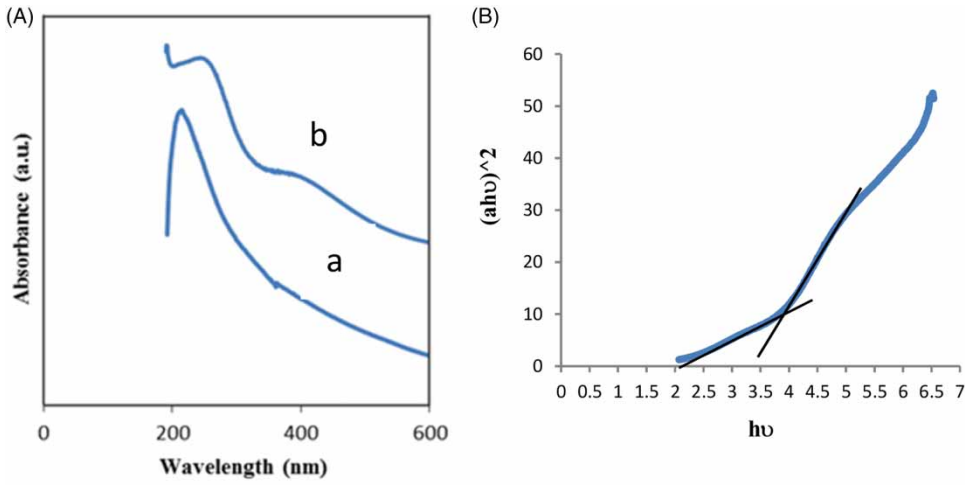

Figure 4 | (A) UV-vis spectra of CoZnAl-LDH (a) and CoZnAl-MMO (b) (B) and estimating the band gap of CoZnAl-MMO.

Figure 4(b) shows the relationship between $(ahv)^2$ and hv. The band gap energy of CoZnAl-MMO, determined by extrapolating the linear part of the $(ahv)^2$against hv, was about 2.2 and 3.4 eV. The UV-vis spectrum of CoZnAl-LDH proved that it is not active in the visible range.

Adsorption and photocatalytic performance

AO7 was used as the model pollutant to study the samples' adsorption and photocatalytic properties. The experiments were done over a pH range of 4.5 to 8. Figures 5 and 6 show the effects of initial pH on the proportional removal of AO7 over time. The AO7 removal efficiency by LDH declined with rising pH, showing that AO7 is adsorbed easily on the LDH surface in neutral or acid conditions.

Figure 7 shows that the pH_{pzc} of LDH and MMO is 5.6 and 5.8, respectively. At $pH < pH_{pzc}$, the surface charge is positive, causing electrostatic attraction between anionic AO7 and the CoZnAl-LDH surface (Wang & Wang 2008). But at $pH > pH_{pzc}$, good adsorption capacity was observed for LDH, while experiments indicated that, contrary to expectation, MMO's proportional removal of AO7 increased with increasing pH. There should, therefore, be another adsorption mechanism at pHs exceeding pH_{pzc}. It is possible that AO7's $-SO_3^-$ group assisted the

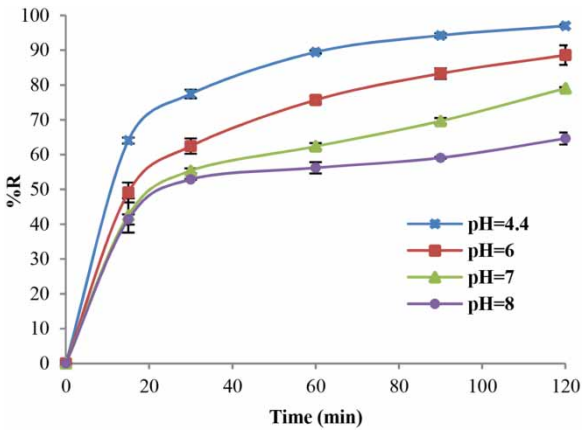

Figure 5 | Effect of pH on AO7 adsorption efficiency using CoZnAl-LDH (adsorbent dose = 0.01 g, initial dye concentration = 40 mg/L).

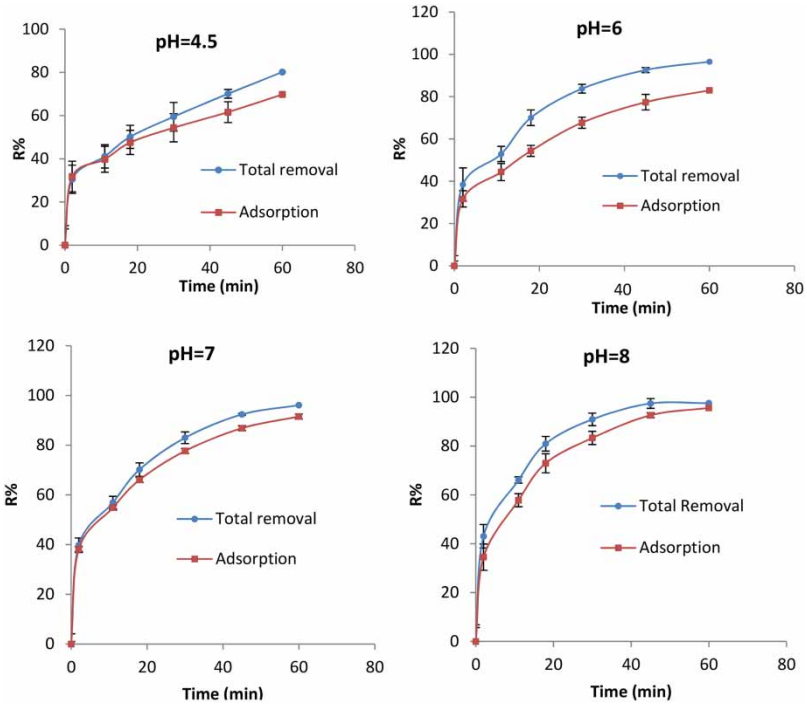

Figure 6 | Effect of pH on AO7 removal efficiency using CoZnAl-MMO (adsorbent dose = 0.01 g, initial dye concentration = 40 mg/L).

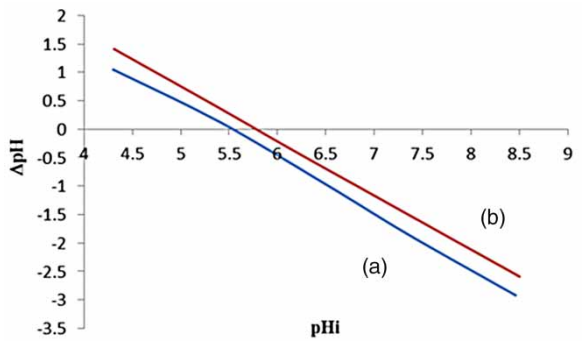

Figure 7 | Plot of ΔpH vs. initial pH to determine the PZC of CoZnAl-LDH (a) and CoZnAl-MMO (b) (T = 25 °C, agitation rate = 120 rpm, t = 24 hr).

creation of a hydrogen bond between adsorbent and dye. At higher pHs, the hydroxyl groups' concentration is higher on the surface, and the possibility of hydrogen bond formation increases. Li *et al.* (2017) discussed hydrogen bond formation between MoS_2/CoAl-LDH/HCF and Congo red in this regard.

For further verification of the adsorption mechanism, the XRD analyses of the LDHs before and after dye adsorption are presented in Figure 8. After AO7 adsorption, the LDH XRD pattern is almost unchanged, thus, demonstrating that the dye was adsorbed on the external surface of the CoZnAl-LDH rather than between its layers.

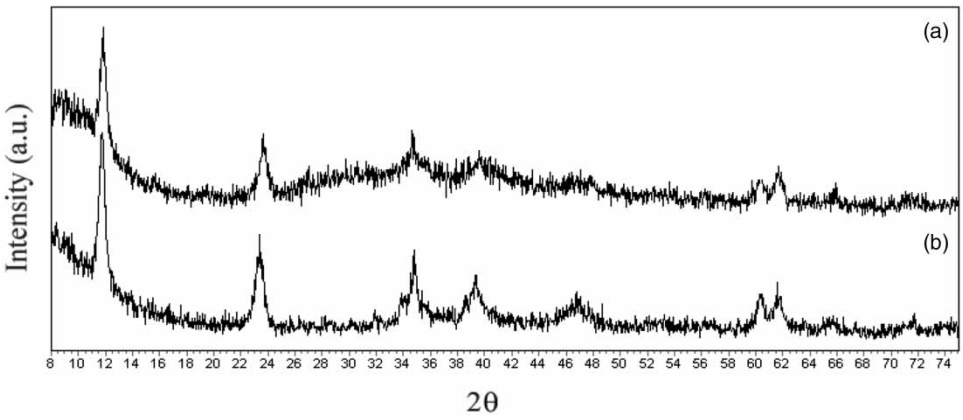

Figure 8 | XRD patterns of CoZnAl-LDH before (a) and after (b) adsorption.

A marked increase in AO7 adsorption was observed for MMO compared with LDH. During calcination, the blocked anions (mainly Cl^-) leave the LDH structure. When MMO is placed in a solution containing anions, it is possible for anions and water molecules to enter between its layers; this phenomenon is called reconstruction (Cheng *et al.* 2009). On this basis, AO7 can be adsorbed either on MMO's external surface or intercalated between its layers, increasing AO7 adsorption efficiency.

The photocatalytic activity of CoZnAl-MMO falls at higher pHs – see Figure 9. This may be due to the fact that in acidic conditions, anionic AO7 is adsorbed directly onto the positive MMO surface and destroyed. The concentration of OH^- ions rises with increasing pH, and these ions compete with AO7 to occupy the LDH surface (Ayoubi-Feiz *et al.* 2014). Interaction between dye and photocatalyst is thus reduced. The MMO degraded 5.15 mg/L of AO7 at pH = 6 within an hour.

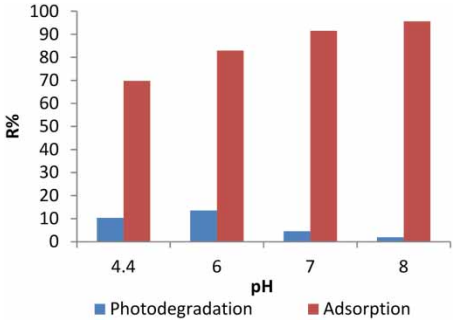

Figure 9 | Effect of pH on AO7 removal efficiency using CoZnAl-MMO after 60 min contact time.

Adsorption isotherm analysis

Three adsorption isotherms, Langmuir, Freundlich, and Temkin were studied by fitting the equilibrium data.

The Langmuir isotherm relates to homogeneous adsorption and monolayer surface coverage. The linearized form of the Langmuir model is described in Equation (4) (Chen *et al.* 2013):

$$\frac{C_e}{q_e} = \frac{1}{q_m K_L} + \frac{C_e}{q_m} \tag{4}$$

where C_e is the equilibrium concentration of AO7 (mg/L), q_e the amount of AO7 adsorbed in equilibrium (mg/g), q_m the maximum adsorption capacity (mg/g), and K_L the Langmuir constant. The dispersion coefficient (R_L) is the Langmuir isotherm's most important factor and is expressed in Equation (5):

$$R_L = \frac{1}{(1 + K_L C_0)} \tag{5}$$

where K_L is the Langmuir constant and C_0 the substance's initial concentration (mg/L). The value of R_L indicates whether AO7 adsorption is unfavorable ($R_L > 1$), favorable ($0 < R_L < 1$), linear ($R_L = 1$), or irreversible ($R_L = 0$).

The Freundlich isotherm determines heterogeneous and multilayer adsorption. The model's logarithmic form is given in Equation (6) (Crini *et al.* 2007):

$$Lnq_e = LnK_F + \frac{1}{n} LnC_e \tag{6}$$

where q_e and C_e are the amounts of adsorbed substance (mg/g) and the concentration of AO7 (mg/L) at equilibrium, respectively, K_F the Freundlich constant (L/g) related to adsorption capacity, and $1/n$ the heterogeneity factor. If $1 < n < 10$, adsorption is favorable.

The Temkin isotherm model defines an interaction between adsorbate and adsorbent, and is described in Equation (7) (Chen *et al.* 2013):

$$q_e = BLnA + BLnC_e \tag{7}$$

where $B = RT/b$, b is the Temkin constant (J/mol), R the gas constant (8.314 J/mol.k), T the absolute temperature (K), and A the Temkin isotherm constant (L/g).

Table 3 shows the parameters obtained from the three isotherms. The R^2 value for the Langmuir isotherm is the closest to one, suggesting that AO7 adsorption onto CoZnAl-LDH and CoZnAl-MMO should be monolayer. The R_L value was between 0 and 1, indicating that adsorption is favorable. It is also noted that AO7's maximum adsorption capacities onto as-prepared LDH and MMO were 243.90 and 526.32 mg/g, respectively – substantial amounts among common adsorbents.

Table 3 | Parameters for three isothermal models of AO7 adsorption onto the LDH and MMO

Model	Parameters	CoZnAl-LDH	CoZnAl-MMO
Langmuir	R^2	0.997	0.998
	R_L	$0 < R_L < 1$	$0 < R_L < 1$
	Q_m (mg/g)	243.9024	526.32
Freundlich	R^2	0.8023	0.904
Temkin	R^2	0.7803	0.8778

Table 4 clearly shows that the adsorption capacities of CoZnAl-LDH and especially CoZnAl-MMO for AO7 are much higher than those of other adsorbents used to date. In this context, the simplicity and low cost of preparation are major benefits of CoZnAl-LDH and MMO with respect to AO7 removal from water.

Adsorption kinetics study

In order to further study the adsorption properties of AO7 onto CoZnAl-LDH and MMO, the experimental results were fitted to pseudo-first-order and pseudo-second-order models.

The pseudo-first-order kinetic model is expressed in Equation (8) (Azizian 2004):

$$Ln(q_e - q_t) = Lnq_e - k_1 t \tag{8}$$

Table 4 | Maximum adsorption capacity comparisons of CoZnAl-LDH and CoZnAl-MMO with other adsorbents

Adsorbent	Adsorption capacity (mg/g)	Reference
SBG	30.5	Silva *et al.* (2004)
Activated carbon	0.4	Aber *et al.* (2007)
Azolla rongpong	77	Padmesh *et al.* (2006)
Canola stalks	25	Hamzeh *et al.* (2012)
MC	0.19	Lim *et al.* (2013)
CoZnAl-LDH	243.9	This study
CoZnAl-MMO	526.3	This study

where q_e and q_t (both mg/g) are the amounts of AO7 adsorbed at equilibrium and time t, respectively, and k_1 (1/min) the adsorption rate constant.

The pseudo-second-order kinetic model is described in Equation (9) (Ho & McKay 1999):

$$\frac{t}{q_t} = \frac{1}{k_2 q_e^2} + \frac{1}{q_e} t \tag{9}$$

where k_2 (g/mg.min) is the adsorption rate constant.

Table 5 shows the parameters obtained from two kinetic models. AO7 adsorption on CoZnAl-LDH and CoZnAl-MMO follows the pseudo-second-order and pseudo-first-order equations, respectively. In both cases R^2 value is close to one.

Table 5 | Kinetic constants for AO7 adsorption onto the LDH and MMO adsorbents

CoZnAl-LDH AO7 concentration (mg/L)	k_2	R^2	CoZnAl-MMO AO7 concentration (mg/L)	k_1	R^2
30	0.004965	0.9977	70	0.0195	0.9826
40	0.004534	0.998	90	0.0131	0.9842
60	0.003823	0.994	110	0.0099	0.9864

CONCLUSION

CoZnAl-LDH, which has a high specific surface, was synthesized by co-precipitation and showed good AO7 adsorption capacity. CoZnAl-MMO was obtained by calcining the initial LDH and demonstrated excellent adsorption performance. XRD, SEM and EDS analyses showed that sample synthesis was successful. The BET results showed that the samples had high specific surfaces, which makes them function efficiently as adsorbents. Calculation of the band gap energy of CoZnAl-MMO and the experimental results both showed that CoZnAl-MMO can be active in visible light. Kinetic studies confirmed the pseudo-second-order and pseudo-first-order AO7 adsorption kinetics on the CoZnAl-LDH and CoZnAl-MMO, respectively. AO7 adsorption on both LDH and MMO fits the Langmuir isotherm model.

ACKNOWLEDGEMENTS

The authors are grateful to the University of Tabriz for financial and other supports.

DATA AVAILABILITY STATEMENT

All relevant data are included in the paper or its Supplementary Information.

REFERENCES

Abdollahi, B., Shakeri, A., Aber, S. & Sharifi-Bonab, M. 2018 Simultaneous photodegradation of acid orange 7 and removal of Pb^{2+} from polluted water using reusable clinoptilolite–TiO_2 nanocomposite. *Research on Chemical Intermediates* **44**(3), 1505–1521.

Aber, S., Daneshvar, N., Soroureddin, S. M., Chabok, A. & Asadpour-Zeynali, K. 2007 Study of acid orange 7 removal from aqueous solutions by powdered activated carbon and modeling of experimental results by artificial neural network. *Desalination* **211**(1–3), 87–95.

Ahmed, M. & Mohamed, A. 2017 An efficient adsorption of indigo carmine dye from aqueous solution on mesoporous Mg/Fe layered double hydroxide nanoparticles prepared by controlled sol-gel route. *Chemosphere* **174**, 280–288.

Ayoubi-Feiz, B., Aber, S., Khataee, A. & Alipour, E. 2014 Electrosorption and photocatalytic one-stage combined process using a new type of nanosized TiO_2/activated charcoal plate electrode. *Environmental Science and Pollution Research* **21**(14), 8555–8564.

Azizian, S. 2004 Kinetic models of sorption: a theoretical analysis. *Journal of Colloid and Interface Science* **276**(1), 47–52.

Chen, J., Ahmad, A. & Ooi, B. 2013 Poly (N-isopropylacrylamide-co-acrylic acid) hydrogels for copper ion adsorption: equilibrium isotherms, kinetic and thermodynamic studies. *Journal of Environmental Chemical Engineering* **1**(3), 339–348.

Cheng, X., Huang, X., Wang, X., Zhao, B., Chen, A. & Sun, D. 2009 Phosphate adsorption from sewage sludge filtrate using zinc–aluminum layered double hydroxides. *Journal of Hazardous Materials* **169**(1), 958–964.

Crini, G., Peindy, H. N., Gimbert, F. & Robert, C. 2007 Removal of CI basic Green 4 (Malachite Green) from aqueous solutions by adsorption using cyclodextrin-based adsorbent: kinetic and equilibrium studies. *Separation and Purification Technology* **53**(1), 97–110.

Davis, E. & Mott, N. 1970 Conduction in non-crystalline systems V. Conductivity, optical absorption and photoconductivity in amorphous semiconductors. *Philosophical Magazine* **22**(179), 0903–0922.

Hamzeh, Y., Ashori, A., Azadeh, E. & Abdulkhani, A. 2012 Removal of Acid Orange 7 and Remazol Black 5 reactive dyes from aqueous solutions using a novel biosorbent. *Materials Science and Engineering: C* **32**(6), 1394–1400.

Ho, Y.-S. & McKay, G. 1999 Pseudo-second order model for sorption processes. *Process Biochemistry* **34**(5), 451–465.

Klemkaite, K., Prosycevas, I., Taraskevicius, R., Khinsky, A. & Kareiva, A. 2011 Synthesis and characterization of layered double hydroxides with different cations (Mg, Co, Ni, Al), decomposition and reformation of mixed metal oxides to layered structures. *Open Chemistry* **9**(2), 275–282.

Kong, L., Tian, Y., Wang, Y., Li, N., Liu, Y., Pang, Z., Huang, X., Li, M., Zhang, J. & Zuo, W. 2019 Periclase-induced generation of flowerlike clay-based layered double hydroxides: a highly efficient phosphate scavenger and solid-phase fertilizer. *Chemical Engineering Journal* **359**, 902–913.

Kovanda, F. & Jirátová, K. 2011 Supported layered double hydroxide-related mixed oxides and their application in the total oxidation of volatile organic compounds. *Applied Clay Science* **53**(2), 305–316.

Li, H., Li, J., Xu, C., Yang, P., Ng, D. H., Song, P. & Zuo, M. 2017 Hierarchically porous MoS_2/CoAl-LDH/HCF with synergistic adsorption-photocatalytic performance under visible light irradiation. *Journal of Alloys and Compounds* **698**, 852–862.

Li, J., Xu, Y., Ding, Z., Mahadi, A. H., Zhao, Y. & Song, Y.-F. 2020 Photocatalytic selective oxidation of benzene to phenol in water over layered double hydroxide: a thermodynamic and kinetic perspective. *Chemical Engineering Journal* **388**, 124248.

Lim, C. K., Bay, H. H., Neoh, C. H., Aris, A., Majid, Z. A. & Ibrahim, Z. 2013 Application of zeolite-activated carbon macrocomposite for the adsorption of Acid Orange 7: isotherm, kinetic and thermodynamic studies. *Environmental Science and Pollution Research* **20**(10), 7243–7255.

Mahdizadeh, F. & Aber, S. 2015 Treatment of textile wastewater under visible LED lamps using CuO/ZnO nanoparticles immobilized on scoria rocks. *RSC Advances* **5**(92), 75474–75482.

Morimoto, K., Tamura, K., Iyi, N., Ye, J. & Yamada, H. 2011 Adsorption and photodegradation properties of anionic dyes by layered double hydroxides. *Journal of Physics and Chemistry of Solids* **72**(9), 1037–1045.

Mostafa, M. S., Bakr, A.-S. A., El Naggar, A. M. & Sultan, E.-S. A. 2016 Water decontamination via the removal of Pb (II) using a new generation of highly energetic surface nano-material: $Co^{+2}Mo^{+6}$ LDH. *Journal of Colloid and Interface Science* **461**, 261–272.

Padmesh, T., Vijayaraghavan, K., Sekaran, G. & Velan, M. 2006 Application of Azolla rongpong on biosorption of acid red 88, acid green 3, acid orange 7 and acid blue 15 from synthetic solutions. *Chemical Engineering Journal* **122**(1), 55–63.

Patra, S., Roy, E., Madhuri, R. & Sharma, P. K. 2016 Agar based bimetallic nanoparticles as high-performance renewable adsorbent for removal and degradation of cationic organic dyes. *Journal of Industrial and Engineering Chemistry* **33**, 226–238.

Rathee, G., Singh, N. & Chandra, R. 2020 Simultaneous elimination of dyes and antibiotic with a hydrothermally generated NiAlTi layered double hydroxide adsorbent. *ACS Omega* **5**(5), 2368–2377.

Silva, J. P., Sousa, S., Rodrigues, J., Antunes, H., Porter, J. J., Gonçalves, I. & Ferreira-Dias, S. 2004 Adsorption of acid orange 7 dye in aqueous solutions by spent brewery grains. *Separation and Purification Technology* **40**(3), 309–315.

Speed, D. 2016 Environmental aspects of planarization processes. In: *Advances in Chemical Mechanical Planarization (CMP)*, (S. Babu, ed.). Woodhead Publishing, Sawston, Cambs, pp. 229–269.

Thommes, M., Kaneko, K., Neimark, A. V., Olivier, J. P., Rodriguez-Reinoso, F., Rouquerol, J. & Sing, K. S. 2015 Physisorption of gases, with special reference to the evaluation of surface area and pore size distribution (IUPAC technical report). *Pure and Applied Chemistry* **87**(9–10), 1051–1069.

Wang, L. & Wang, A. 2008 Adsorption properties of Congo red from aqueous solution onto N, O-carboxymethyl-chitosan. *Bioresource Technology* **99**(5), 1403–1408.

Xu, Z. P., Zhang, J., Adebajo, M. O., Zhang, H. & Zhou, C. 2011 Catalytic applications of layered double hydroxides and derivatives. *Applied Clay Science* **53**(2), 139–150.

Xu, J., Gai, S., He, F., Niu, N., Gao, P., Chen, Y. & Yang, P. 2014 Reduced graphene oxide/$Ni_{1-x}Co_x$ Al-layered double hydroxide composites: preparation and high supercapacitor performance. *Dalton Transactions* **43**(30), 11667–11675.

Yu, J., Lu, L., Li, J. & Song, P. 2016 Biotemplated hierarchical porous-structure of ZnAl-LDH/$ZnCo_2O_4$ composites with enhanced adsorption and photocatalytic performance. *RSC Advances* **6**(16), 12797–12808.

First received 5 April 2021; accepted in revised form 30 July 2021. Available online 16 August 2021